Helsinki University of Technology Institute of Mathematics Research Reports
Teknillisen korkeakoulun matematiikan laitoksen tutkimusraporttisarja
Espoo 1999 A410

# BOUNDED TRIANGULAR AND KAGOM ICE

Kari Eloranta

Helsinki University of Technology
Department of Engineering Physics and Mathematics
Institute of Mathematics

**Kari Eloranta**: Bounded Triangular and Kagomé Ice; Helsinki University of Technology Institute of Mathematics Research Reports A410 (1999).

**Abstract:** *The long range boundary dependency prevailing in the ice-model on the square lattice extends to a few other discrete planar set-ups. Here we present the findings in the context of the 20-vertex model on triangular lattice and 18-vertex rule on the Kagomé lattice. The critical connectivity results that guarantee that configurations can be generated using the simplest and most efficient local actions hold in these contexts. Boundary height is of central importance in determining the entropy and geometry of the template zone inside the domain.*

**AMS subject classifications:** 52C20, 68Q80, 82C20.

**Keywords:** 18/20-vertex model, ice model, Kagomé lattice, propabilistic cellular automaton.

ISBN 951-22-4408-X
ISSN 0784-3143
Edita, Espoo, 1999

Helsinki University of Technology
Department of Engineering Physics and Mathematics
Institute of Mathematics
P.O. Box 1100, 02015 HUT, Finland
email: *math@hut.fi*
downloadables: *http://www.math.hut.fi/*

author's email: *eloranta@janus.hut.fi*

# 0. Introduction

The 20-vertex model on the triangular lattice and the 18-vertex model on the Kagomé lattice are analogs ice model on the square lattice. In this note we investigate the basic properties of their bounded versions. This serves two purposes. Firstly this complements the various studies of the infinite unbounded models and answers the question on the influence of the boundary posed by Kasteleyn ([K]). Secondly we hope to contribute to the unification of the theories of lattice statistical mechanics, higher dimensional symbolic dynamics and tilings that has been worked on for some time now (starting from [CL], [T] etc.).

Our results show that the 20-vertex model on triangular lattice, 18-vertex model on Kagomé lattice and square ice can be analyzed with similar means. They have analogous cycle structure which ultimately facilitates their computation with simple and efficient algorithms. Height works in the same way in these models and the boundary effects it forces are qualitatively similar in these three models. There is sharp a demarcation of temperate and frozen subdomains akin to the Arctic Circle Phenomenon in dominoes ([JPS]). The lattice independence is in a notable contrast with e.g. the hard hexagon and hard square models where the underlying lattice (triangular or square) forces completely different analysis ([B]). Because of the close connections between the bounded 6/18/20-vertex models we refer for the results on six-vertex model in [E] and concentrate here on the novel features. We make however an effort to make this paper self-contained so that the reader can grasp the main ideas and results if not all the proofs just from here.

# 1. Set-up

**Vertex-models** of the Statistical Mechanics can be defined on various lattices, in the planar case most commonly on square, triangular, hexagonal and Kagomé-lattices. In these models all the nearest neighbor lattice sites are connected with arrows. Their global ensemble of orientations defines the configuration.

**Definition 1.1.:** *A* **vertex configuration** *at a point on the triangular lattice is* **legal** *for the* **20-vertex rule** *if there are three incoming and three outgoing arrows at that lattice point. Similarly a vertex configuration is legal for the* **18-vertex rule** *on the Kagomé lattice if there are two incoming and two outgoing arrows. If*

*there is a legal vertex configuration at every lattice site on the triangular/Kagomé lattice the arrow configuration is legal for the* **20/18-vertex model.**

**Remarks: 1.** In the square lattice case the **six-vertex rule** accepts vertices with two incoming and two outgoing arrows. It is called the **ice-rule** because of its physical interpretation (see [L]). Although this physical interpretation does not carry over to the set-up in the Definition, for simplicity we call those rules **ice-type.**
**2.** A rule of this kind necessarily requires even vertex degree. Hence in the planar case e.g. hexagonal or octagon-square-lattice are not compatible with the rule. Among the lattices that arise from the 11 Archimedean tilings only square, triangular, Kagomé and one exotic lattice (of type (3.4.6.4), see [GS]) are of even vertex degree.

The possible vertex configurations together with their multiplicities (accounting rotations and reflections) are as indicated in Figure 1., triangular on the left, Kagomé on the right. The names in the Definition refer to the total number of possible vertex configurations.

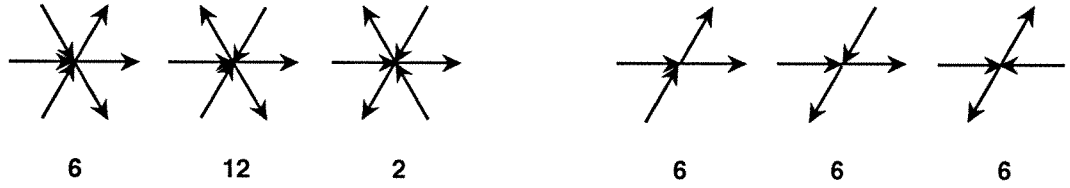


Figure 1a, b. Vertex configurations and their multiplicities.

We study these models on a hexagonal domain. A **$N$-hexagon** in the case of the triangular lattice is a domain which is oriented along the lattice axes with $N$ boundary arrows along each edge, $N$ even. Or equivalently we can require that along each edge there are $N/2$ lattice sites with all six arrows attached to them. Figure 2a. illustrates the area around leftmost corner of such hexagon (the boundary will have six-fold symmetry). The **boundary arrows**, $6N - 6$ in total, are rendered bold. They will be fixed and the main problem will be determining when and how the interior arrows (lighter) can be arranged into a legal configuration.

The other simple and natural domain shapes on the lattice, a unilateral triangle and a rhombus turn out to be somewhat restrictive due to the acute corners. On

the hexagonal domain we will be able to illustrate both "frozen " and "temperate" configurations and their coexistence as in the diamond in square lattice case ([E]).

The dual lattice of the triangular lattice is the hexagonal lattice. Every lattice site is the center of a minimal (unit) hexagon the boundary of which we should think having clockwise orientation. By the 20-vertex rule the total **flux** across this boundary is zero (ingoing arrow counts $+1$, outgoing $-1$). Consider the maximal dual lattice loop on the domain, the boundary loop (the dual lattice edges of this loop still cross arrows in the $N$-hexagon). It is the sum of all the directed unit hexagons in the dual lattice inside the domain. Hence if the configuration inside the domain is legal then the flux across the boundary loop vanishes.

In the Kagomé-lattice $N$-hexagon has $N$ lattice sites and $N/2$-arrows along each edge. Figure 2c. illustrates the leftmost corner of such hexagon. The bold arrows are the fixed boundary arrows. Because of the ice-rule the flux around each lattice point vanishes in this set-up as well. Therefore a legal fill-in of a hexagon will have zero boundary flux.

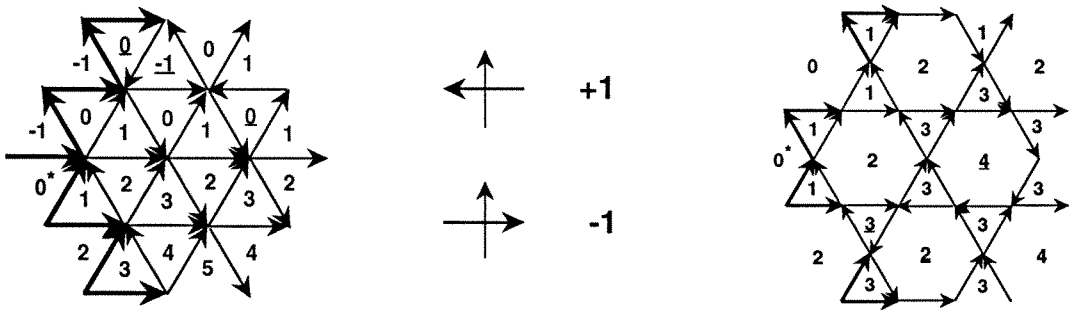


Figure 2a, b, c. Crossing rule and sample configurations with heights.

Let $C$ be the set of legal ice configurations on a given triangular lattice hexagon and let $D$, the **dual cover**, denote the finite subset of the hexagonal lattice that has the property that an edge connecting a nearest neighbor pair of vertices from $D$ crosses an arrow in $c \in C$.

The **height**, $h : C \times D \to \mathbf{Z}$, is an extremely useful function in analyzing ice-type models. Its increments on $D$ are defined by the crossing rule in Figure 2b. The light arrow indicates the edge on the dual lattice that we move along and the bold marks the configuration arrow. The rules apply in all possible rotations. Note that height around a closed loop in $D$ vanishes (since this is the same as computing

the flux across that loop). Hence $h$ is independent of the path along which it was computed. To be unique it needs to be specified at one **base point** which we choose to be the leftmost dual lattice point (starred). In Figure 2a. we have indicated the heights with the choice that at the base point height vanishes.

The dual of the Kagomé lattice is the rhombus-lattice (corresponding to Laves tiling of type [3.6.3.6]). The definition of height on it as above is straightforward and we have indicated its values in Figure 2c.

The three cases when height increases/decreases at a maximal rate or alternates in value along a path in the dual lattice will be important in later considerations. As the boundary specification will be critical we have also chosen to illustrate this on the boundaries in Figure 2. The boundary arrows in the lower halfs of the samples in both triangular and Kagomé-case are in an ensemble of maximal **tilt** as we follow the boundary. The upper half of the boundary arrows illustrate the alternating case. Subsequently we refer these special arrangements as having tilt $\pm 1$ or 0.

## 2. Connectivity

The ice-type local arrow parity implemented in Definition 1.1. has far reaching consequences on the global structure of the configuration ensembles independent of the underlying lattice. We now elaborate on this utilizing as well as extending the results in the square lattice case in [E].

Consider a legal triangular or Kagomé ice configuration. Suppose that we can find a closed unidirectional path of configuration arrows in it (or a path from infinity to infinity). Reversing this directed cycle i.e. flipping every arrow on the cycle results in an other legal configuration since the rule at each vertex is respected. Existence of a directed cycle is therefore related to the non-uniqueness of the fill-in: a boundary arrangement of arrows that allows a fill-in which has an off-boundary cycle allows in fact multiple fill-ins.

**Definition 2.1.:** *Call the smallest lattice triangle a* **1-triangle**. *The orientation* $\triangle$ *is* **even** *and* $\triangledown$ *is* **odd**. *On the Kagomé lattice we have additionally a minimal hexagon, a* **1-hexagon**. *If these are unidirectional we call them* **1-cyles**.

In the case of a finite cycle one can show by utilizing flux as in the square lattice case (see [E]) that in fact

**Proposition 2.2.:** *A unidirectional cycle always encloses a 1-cycle.*

We say that a cycle is **off-boundary** if it does not contain any of the (fixed) boundary arrows. Define a bounded **frozen** configuration to be one without off-boundary 1-cycles. Its opposite is the **temperate** configuration which we define as one having a directed cycle boundary.

In Figure 2a. and c. sample configurations contain 1-cycles – they are the ones with height underlined. The samples are typical in the sense that neither has a cycle boundary yet they have 1-cycles. Except for special boundary configurations the fill-in will exhibit a coexistence of frozen and temperate subdomains.

Related to the 1-cycles there is a simple but useful notion which we will need in the proof of our main theorem. In Figure 3. the infinite wedges $C_i$ rooted at the vertices of the 1-cycles are called **contact sectors**. For the triangle oriented upside down we reflect the wedges and for 1-hexagon we have for clarity indicated only the odd sectors.

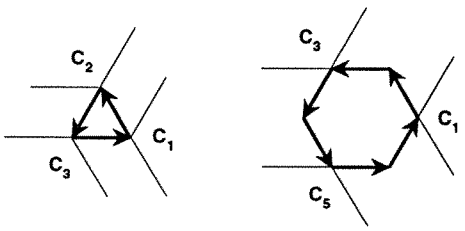


Figure 3a, b. Contact sectors.

The main result that the cycle structure of configurations implies for both triangular and Kagomé ice is the following.

**Theorem 2.3.:** *The set of configurations with common boundary arrows on a N-hexagon is connected under 1-cycle reversals i.e. two such configurations can be transformed to each other with a finite sequence of 1-cycle reversals.*

**Proof:** The argument is similar "lexicographic sweep" as in the square case with some refinements (see [E]). When we arrive to a lattice point $l$ where there is the next mismatch between the two configurations under comparison, the situation in

triangular lattice looks like in Figure 4a. $L$ denotes the "front" above which all vertex configurations in the two configurations match. In the Kagomé case we may encounter three different arrangements, two of which are in Figures 4b, c. (the third is like the rightmost, only rotated 60 degrees clockwise).

Consider first the case on triangular lattice. The three arrows $a - c$ cannot all be in or all out since in that case there cannot be a mismatch. So among arrows $1 - 3$ there is a 2-1 or 1-2 division between ingoing and outgoing arrows. Hence we can always find among them a pair ($(1,2)$, $(1,3)$ or $(2,3)$), same pair on both configurations, so that the arrows in the pairs are unidirectional but oriented opposite in the two configurations. One then extends these 2-paths to closed off-boundary cycles, same cycles but with opposite orientations, on the two configurations.

Pick one of the configurations e.g. the one with clockwise oriented cycle, $O_1$. By Proposition 2.2. inside it there is at least one 1-cycle of some type. Denote their collection by $\{C_i\}$. Choose two of its contact sectors in such a way that they do not overlap and do not contain the point of mismatch $l$. One can easily show that it is possible to find two directed paths, one in each of the contact sectors, which connect the 1-cycle to $O_1$. Moreover the orientations of these paths are such that a new clockwise directed cycle is formed that passes through $l$, along the edge of the 1-cycle and is contained in the domain bounded by $O_1$. This construction is done to all of the 1-cycles inside $O_1$. Finally define the natural minimal directed cycle along these new cycles inside $O_1$ and call it $\tilde{O}_1$.

Now some the 1-cycles inside $O_1$ are on the boundary of the $\tilde{O}_1$ and none are strictly in its interior. By reversing these cycles if necessary we obtain a new directed cycle $O_2$ with the property that all of the 1-cycles $\{C_i\}$ are left outside it. Moreover $O_2$ encloses a strictly smaller area than $O_1$, all inside it.

Applying the argument above to $O_2$, $O_3$ and so on finally forces a 1-cycle that has $l$ as its vertex. Hence we correct a mismatch at $l$. Note that if the path $O_1$ involved the pair $(1,3)$ we need a second application of this argument, now to a loop through $(1,2)$ or $(2,3)$, whichever pair is still mismatched in the two configurations. After this all arrows at $l$ match and the front $L$ moves to the next lexicographic location to check for a mismatch.

For the Kagomé lattice the argument is similar. Whether the 1-cycle is a 1-triangle or 1-hexagon makes no difference except in the choice of the contact sectors.

Note that for Kagomé lattice (as well as square lattice) one pass of the argument above for each $l$ is sufficient to correct the mismatch. ∎

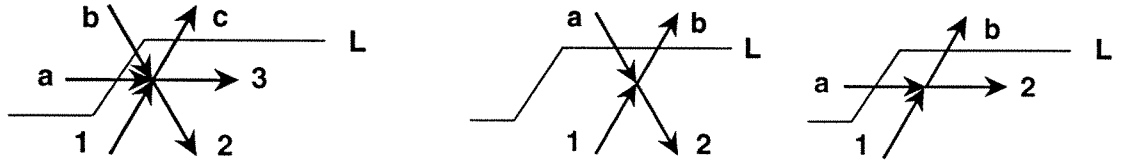


Figure 4a, b, c. Vertex configuration mismatch.

**Remark:** Since the "sweep" is a rather general procedure to deal with the configuration, the result will hold for more general domain geometries as well. But since our presentation is geared towards analyzing boundary dependency in a hexagonal domain we refrain from pursuing this.

The result is optimal: no smaller set of elementary moves will guarantee connectivity. This follows simply from counterexamples.

Suppose that we have a configuration on the triangular lattice where each of the lattice arrows is directed either towards 1, 3 or 5 o'clock. Then reverse all the arrows on one of the 1 o'clock and 5 o'clock lattice lines. Cut a $N$-hexagon out from this so that the intersection of these lattice lines is at the center. The patch that we see at the center of the hexagon looks like Figure 5a.

Reversing the 1-triangle at $C$ will obviously not affect the boundary arrows i.e. we get another configuration, call it $\tilde{H}$, compatible with the boundary configuration. If we are subsequently only allowed to act with $\triangle$-reversals there will be only two such triangles to work on, the one at $T$ in $\tilde{H}$ and the one below $C$. But it is easy to see that reversing these and any other directed $\triangle$-cycles will never yield a directed cycle outside the two acute wedges defined by the bold lines. Hence two sides of $C$ will never be returned to their original orientation.

In the case of Kagomé lattice we generate a configuration as above, this time from arrow lines pointing towards 3, 7 and 11 o'clock. This configuration has has the property that all 1-triangles are directed (see Figure 5b.). If we reverse any one of them, say $C$, the new configuration is compatible with the boundary but still has no directed 1-hexagons. Notice that even if only the reversal of $\bigtriangledown$ is forbidden we are still stuck. Reversing $C$ cannot be undone with $\triangle$-actions and all the 1-hexagons will still remain undirected.

Finally if the configuration is generated in an alternating fashion from arrow-lines to directions 1 and 7, 3 and 9 and 5 and 11 o'clock we can see in it a patch like Figure 5c. If we reverse the 1-hexagon, the 1-triangles around it will become directed but the David's star is isolated from the 1-cycle reversals outside it, so its original orientations cannot be returned.

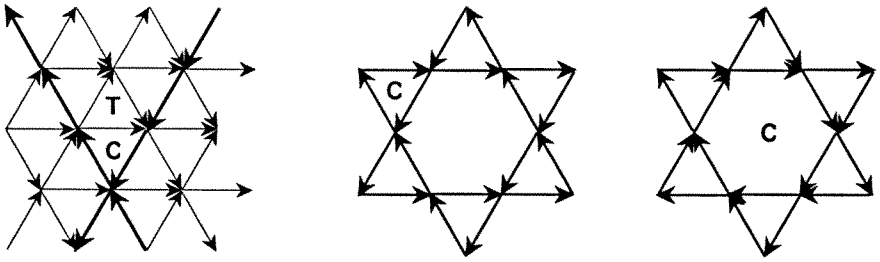


Figure 5a, b, c. Restricted action.

Hence we can conclude from these counterexamples a slight sharpening to the Theorem above.

**Proposition 2.4.:** *The connectivity result of Theorem 2.3. fails if*
*(i) in the triangular lattice case not both types of directed 1-triangles are reversible*
*(ii) in the Kagomé lattice case not all three directed 1-cycle types are reversible.*

# 3. Boundary dependency

Perhaps the most significant consequence of Theorem 2.3. is that it paves the way to efficient generation the configurations with a given boundary configuration. We now proceed in indicating how this is done and then present some simulation results.

The arrows of the triangular lattice can be viewed as an array of either just even or just odd oriented 1-triangles. Call their restrictions to the $N$-hexagon $L_e$ and $L_o$ respectively.

On the triangle arrays we define two local update rules. If an off-boundary even/odd directed 1-cycle is encountered, it is reversed independently with probability 1/2 and also its odd/even nearest neighbor 1-triangles are updated accordingly. These rules immediately give global random maps $F_e$ and $F_o$ which check 1-cycles on $L_e$ and $L_o$ respectively and update the arrow configuration on both. They define a **probabilistic cellular automaton (pca)** action on the configurations.

On the Kagomé lattice we additionally define a local rule reversing a directed 1-hexagon with probability 1/2 and updating the six neighboring 1-triangles. Call its global map $F_h$. The updating sequence $\{F_e, F_h, F_o, F_h\}$ defines the pca cycle.

Given any initial configuration by Theorem 2.3. the pcas above will almost surely generate any configuration compatible with the boundary configuration of the initial one. The choice of probability 1/2 for the flip is for maximal speed. In the Kagomé case the choice of checking the 1-hexagons twice as often as the even/odd triangles, is to the same end.

As with any Monte Carlo scheme we expect this pca action to relax from every initial configuration to the configuration distribution corresponding to the measure of maximal entropy conditioned to the boundary configuration. Hence the configurations that we observe along the orbit of the pca – once it has reached the equilibrium – should be typical to that measure. We do not know of any rigorous relaxation rate result applicable here but in all simulations performed it seemed high and is likely to be exponential.

By **boundary height** of a configuration we mean the restriction of height to the boundary of the dual cover $D$ (see Section 1.). Following this boundary loop we only cross boundary arrows.

Suppose that the boundary height is on each edge of tilt 0 or $\pm 1$. Let the **signature** of the boundary be the six-vector that we get by recording the tilts starting from the base point and circumambulating the boundary of $D$ counterclockwise.

For both triangular and Kagomé lattice the signature $(+1, +1, 0, -1, -1, 0)$ and its cyclic permutations correspond to perfectly ordered configurations. They are frozen i.e. contain no directed 1-cycles.

The signature $(0, 0, 0, 0, 0, 0)$ is the maximally disordered case and the configurations are temperate. Now the boundary arrows form directed paths which are at least the length of the edge. The case where the entire boundary is a directed cycle has this signature and clearly has the largest directed cycle in any hexagon.

The choice $(+1, -1, +1, -1, +1, -1)$ recorded in Figure 6. top left. This height choice leads to the coexistence of frozen and temperate domains. Figure 6. middle left illustrates the even 1-cycle flip distribution on triangular 102-hexagon. Here we have recorded every even 1-triangle reversal during the iterates $13 - 19 \times 10^3$. The rendering is that of their cumulative totals during this period when the system was

already close to equilibrium. Darker cells indicate higher flip activity. The light grey background is just to make the hexagon visible. There is a clear demarcation between corner areas where there is essentially no activity and interior where the flip distribution is fairly uniform.

Figure 6. top right, shows another boundary condition. Each edge is now split in the middle into a segments of maximal tilt $\pm 1$ in an alternating fashion. It is easy to see that this choice in fact freezes a lozenge shaped area at each corner (one of which is indicated). Figure 6, middle right illustrates the cumulative even 1-cycle reversal distribution at equilibrium between iterates $6 - 12 \times 10^3$. In both this and the previous simulation the odd 1-cycles did show an identical distribution.

In the Kagomé case these are the simplest interesting boundary conditions as well. Figure 6. bottom row shows the cumulative cycle counts from iterates $12 - 24 \times 10^3$ and $6 - 12 \times 10^3$ for the two boundary choices (system again essentially at equilibrium). The coarser appearance of the images is due to the fact that the 1-cycle density is now half of that in the triangular case.

The rendering shows both even 1-cycle and 1-hexagon flips. The darker entries at the center indicate the array of triangles. At the center their flip frequency is about five times that for 1-hexagons. Note that if the arrows were laid down independently and with probability $1/2$ to each orientation on a given edge, the ratio of the flip probabilities of an even 1-triangle to a 1-hexagon would be eight. Since our pca checks the 1-hexagons twice as often as even 1-triangles it would generate a flip probability ratio exactly four for that distribution. So the maximally disordered vertex-configurations, the statistics of which we expect to see at the center, are some distance from uniform Bernoulli.

While the fine structure of the interior in Figure 6. depends on the algorithm, the actual arrow distribution at the equilibrium does not. And most importantly the key result, the sharp demarcation of frozen and tempered subdomains akin to the Arctic Circle Theorem is plain in Figure 6.

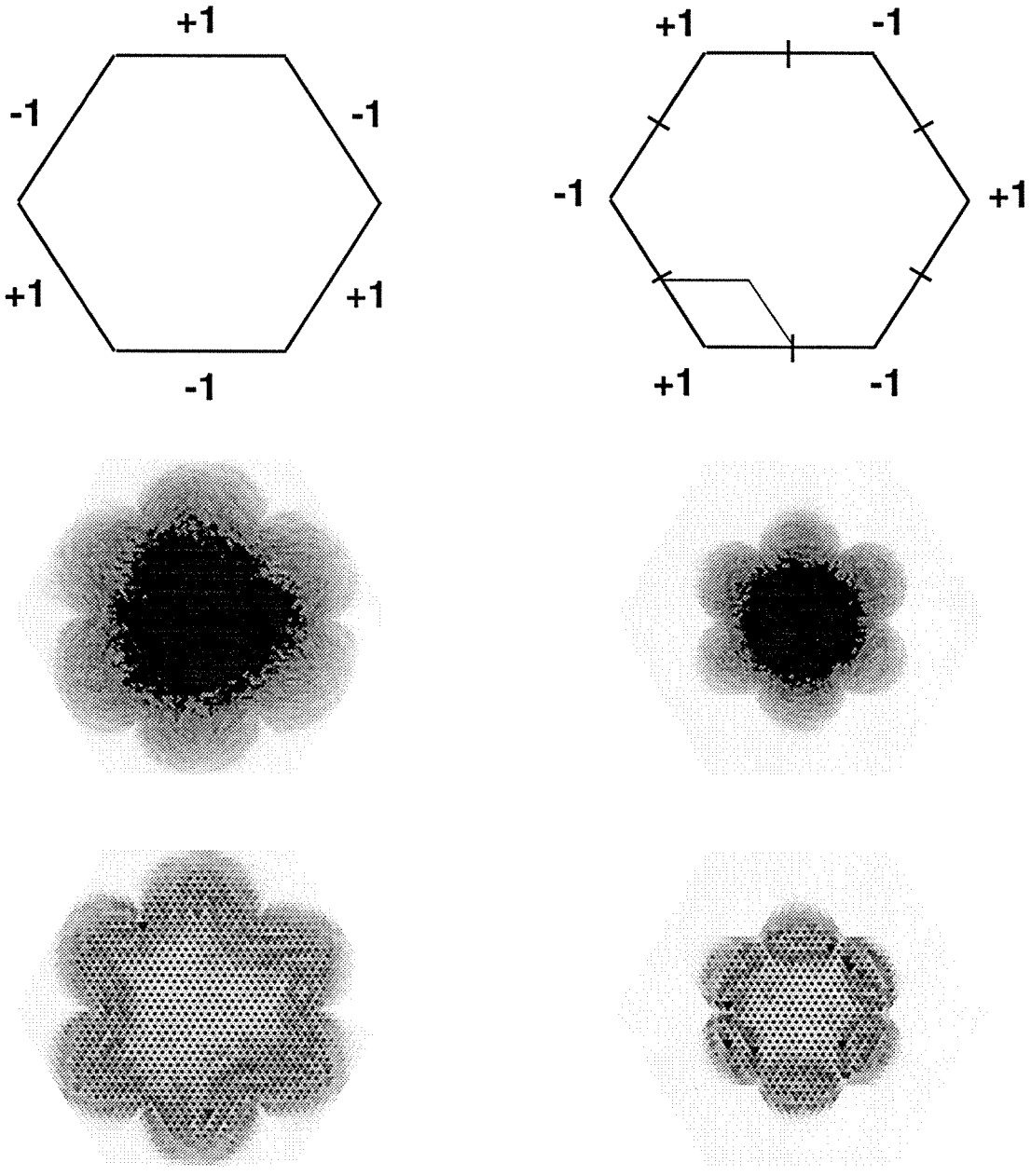


Figure 6. Top: signatures, middle: triangular, bottom: Kagomé.

## Acknowledgement

The author thanks Juha Haataja at CSC for helping in rendering Figure 6.

## References

[B] Baxter, R.J.:*Exactly solvable models in statistical mechanics*, Academic Press, 1982.

[vB] van Beijeren, H.: Exactly solvable model for the roughening transformation of a crystal surface, *Phys. Rev. Lett.*, **38**, 18, pp. 993-996, 1977.

[CL] Conway, J.H., Lagarias, J.C.: Tilings with polyominoes and combinatorial group theory, *J. Combin. Theory*, Ser. A, **53**, pp. 183-208, 1990.

[E] Eloranta, K.: Diamond Ice, to appear in *J. Stat. Phys.*, 1999.

[GS] Grünbaum, B., Shephard, G. C.: *Tilings and patterns*, Freeman, 1987.

[JPS] Jockush, W., Propp, J., Shor, P.: Random domino tilings and the Arctic Circle Theorem, preprint, 1995.

[K] Kasteleyn, P.: The statistics of the dimer on a lattice, I. The number of dimer arrangements on a quadratic lattice. *Physica* **27**, 1209-25, 1961.

[L] Lieb, E.H.: Residual entropy of square ice, *Phys. Rev.*, **162**, 1, pp. 162-172, 1967.

[T] Thurston, W.P.: Conway's tiling groups, *Am. Math. Montly*, pp. 757-773, Oct. 1990.

(continued from the back cover)

A403 Saara Hyvönen and Olavi Nevanlinna
Robust bounds for Krylov method, Nov 1998

A402 Saara Hyvönen
Growth of resolvents of certain infinite matrice, Nov 1998

A400 Seppo Hiltunen
Implicit functions from locally convex spaces to Banach spaces, Jan 1999

A399 Otso Ovaskainen
Asymptotic and Adaptive Approaches to thin Body Problems in Elasticity

A398 Jukka Liukkonen
Uniqueness of Electromagnetic Inversion by Local Surface Measurements, Aug 1998

A397 Jukka Tuomela
On the Numerical Solution of Involutive Ordinary Differential Systems, 1998

A396 Clement Ph., Gripenberg G. and Londen S-O
Hölder Regularity for a Linear Fractional Evolution Equation, 1998

A395 Matti Lassas and Erkki Somersalo
Analysis of the PML Equations in General Convex Geometry, 1998

A393 Jukka Tuomela and Teijo Arponen
On the numerical solution of involutive ordinary differential equation systems, 1998

A392 Hermann Brunner, Arvet Pedas, Gennadi Vainikko
The Piecewise Polynomial Collocation Method for Nonlinear Weakly Singular Volterra Equations, 1997

A391 Kari Eloranta
The bounded Eight-Vertex Model, 1997

A390 Kari Eloranta
Diamond Ice, 1997